Title
Molecular Engineering for Large Open-Circuit Voltage and Low Energy Loss in Around 10% Non-fullerene Organic Photovoltaics

Journal
ACS Energy Letters, 3(4)

ISSN
2380-8195

Authors
He, B
Yang, B
Kolaczkowski, MA
et al.

Publication Date
2018-04-13

DOI
10.1021/acsenergylett.8b00366

Peer reviewed

ajs00 | ACSJCA | JCA10.0.1465/W Unicode | research.3f (R3.6.i12 HF03:4459 | 2.0 alpha 39) 2017/11/27 07:41:00 | PROD-JCAVA | rq_13121507 | 3/28/2018 15:59:22 | 8 | JCA-DEFAULT

ACS Energy Letters

http://pubs.acs.org/journal/aelccp

Molecular Engineering for Large Open-Circuit Voltage and Low Energy Loss in Around 10% Non-fullerene Organic Photovoltaics

Bo He,[†,‡] Bin Yang,*[,†,‡,#] Matthew A. Kolaczkowski,[†] Christopher A. Anderson,[†] Liana M. Klivansky,[†] Teresa L. Chen,[†] Michael A. Brady,[†,§] and Yi Liu*[,†]

[†]The Molecular Foundry, Lawrence Berkeley National Laboratory, Berkeley, California 94720, United States

[#]College of Materials Science and Engineering, Key Laboratory for Micro-Nano Physics and Technology of Hunan Province, Hunan University, Changsha, Hunan 410082, China

[§]Advanced Light Source, Lawrence Berkeley National Laboratory, Berkeley, California 94720, United States

Supporting Information

ABSTRACT: **Recent efforts in organic photovoltaics (OPVs) have been devoted to obtaining low-bandgap non-fullerene acceptors (NFAs) for high photocurrent generation. However, the low-lying lowest unoccupied molecular orbital (LUMO) level in narrow bandgap NFAs typically results in a small energy difference (ΔE_{DA}) between the LUMO of the acceptor and the highest occupied molecular orbital (HOMO) of the donor, leading to low open-circuit voltage (V_{OC}). The trade-off between ΔE_{DA} and photocurrent generation significantly limits the simultaneous enhancement of both V_{OC} and short-circuit current density (J_{SC}). Here, we report a new medium-bandgap NFA, IDTT-T, containing a weakly electron-withdrawing *N*-ethyl thiabarbituric acid terminal group on each end of the indacenodithienothiophene (IDTT) core. When paired with a benchmark low-bandgap PTB7-th polymer donor, simultaneous enhancement of both ΔE_{DA} and absorption spectral coverage was realized. The OPV devices yield a V_{OC} of 1.01 V, corresponding to a low energy loss of 0.57 eV in around 10% efficiency single-junction NFA OPVs. The design demonstrates a working principle to concurrently increase ΔE_{DA} and photocurrent generation for high V_{OC} and PCE in bulk fullerene-free heterojunction OPVs.**

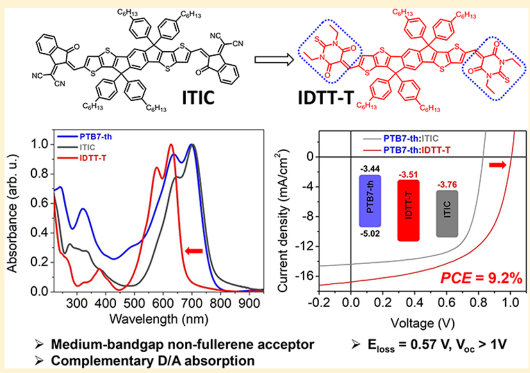

Bulk heterojunction organic photovoltaics (OPVs) have emerged as a promising class of solar cells that offers a potentially low-cost pathway to large-area, lightweight, and mechanically flexible solar panels.[1−3] Steady improvement of device performances has been realized over the past decades, partly owing to the great development of active materials, including both the donor[4] and acceptor materials.[3,4] Engineering of material properties[6−8] is crucial to important device parameters, such as short-circuit current (J_{SC}), open-circuit voltage (V_{OC}), fill factor (FF), and the overall power conversion efficiency (PCE), which are related to the absorption in the visible-near-infrared (NIR) spectrum,[9] relative energy levels,[10,11] and nanoscale phase morphology[12] of the active materials.[13−19] The majority of the OPV devices have employed fullerene derivatives as the electron acceptors for their high electron transport property and excellent crystallization behavior.[13,20,21] Their absorption properties and electronic structures are however less than ideal, which has a limited window for tuning via chemical modification because of the narrow tunability of the fullerene moiety.[22,23] Very recently, an emerging class of non-fullerene acceptors (NFAs) based on low-bandgap fused-ring small molecules has rivaled the dominance of fullerene-based acceptors.[23−31] Their attractive features, such as greater tunability of molecular structures and optoelectronic properties[32−35] and high PCEs that already surpass that of the best fullerene-based single-junction devices,[35−42] have re-established the competitiveness of bulk heterojunction OPVs. Since the seminal work by Zhan et al. that demonstrated the use of 3,9-bis(2-methylene-(3-(1,1-dicyanomethylene)-indanone))-5,5,11,11-tetrakis(4-hexylphenyl)-dithieno[2,3-d:2′,3′-d′]-s-lowindaceno[1,2-b:5,6-b′]-dithiophene (ITIC) as a low-bandgap NFA for OPVs,[32] great progress has been made in the molecular design of NFAs that enable the fabrication of high-efficiency single-junction devices with PCE over 10%.[36,43]

Received: March 7, 2018
Accepted: March 27, 2018

DOI: 10.1021/acsenergylett.8b00366
ACS Energy Lett. XXXX, XXX, XXX−XXX

Despite progress toward approaching the Shockley−Queisser theoretical maximum efficiency, the non-fullerene OPVs still suffer from high energy loss (∼0.7−1.0 eV),[11,15,44,45] which is reflected by the fact that the V_{OC} is generally smaller than half of the optical bandgaps of photoactive molecules in most high-efficiency (PCE ≥ 10%) devices.[11,45] The V_{OC} is a key photovoltaic parameter which is essential to drive portable electronics and consumer electronic devices without employing a complicated tandem structure or resorting to electric utilities.[26,46−52] In principle, the low V_{OC} primarily results from energy level mismatch or internal energy loss during the photoinduced charge-transfer process.[53] The V_{OC} is dependent on the difference between the lowest unoccupied molecular orbital (LUMO) level of the electron acceptor and the highest occupied molecular orbital (HOMO) level of the electron donor ($\Delta E_{DA} = E^{LUMO}_{Acceptor} - E^{HOMO}_{Donor}$).[13] For non-fullerene OPVs, much effort has been devoted to reducing the optical bandgaps of non-fullerene acceptors to extend absorption into the near-infrared portion of the solar spectrum for high photocurrent generation.[33−35,37] This modification generally lowers the LUMO levels, resulting in a decreased ΔE_{DA} and thereby V_{OC} lower than 1 V in most non-fullerene OPVs.[22,33−35,37,38,54] Such a trade-off between ΔE_{DA} and photocurrent generation limits the simultaneous enhancement of both V_{OC} and J_{SC} for high PCEs in non-fullerene OPVs. The medium-bandgap non-fullerene acceptors, although receiving less attention, are a potential remedy to the trade-off: On one hand, their relatively high-lying LUMO levels can increase ΔE_{DA} for high V_{OC}. On the other hand, high J_{SC} may be realized when combined with a variety of known low-bandgap donors, such as the model polymer PTB7-th, to enhance the absorption spectral coverage. However, to the best of our knowledge, such a design principle has been rarely demonstrated.[5]

In this Letter, we demonstrate a proof-of-concept of combining a medium-bandgap non-fullerene acceptor with the low-bandgap donor PTB7-th for high-efficiency OPVs with a high V_{OC}. By adopting an acceptor−donor−acceptor geometry with a weakly electron withdrawing end group, the LUMO energy is increased significantly. This strategy gives rise to an optical bandgap of 2.0 eV that is complementary to electronic energy levels of PTB7-th. The resulting OPVs display a V_{OC} of 1.01 V, which is among the highest in around 10% efficiency single-junction NFA OPVs.

In the design of a medium-gap acceptor IDTT-T, the indacenodithienothiophene (IDTT) core of ITIC was retained on account of its proven ability to facilitate phase separation and crystallization while the strongly electron-withdrawing end groups cyano indone of ITIC were replaced with the weakly electron-accepting *N*,*N*′-diethyl thiobarbituric acid (TBA) (Scheme 1). Molecular modeling based on density function theory (DFT) calculations estimate that this end group substitution would result in a 0.23 eV increase of the optical bandgap and a 0.26 eV increase of the LUMO energy level (Figure 1a). The synthesis of IDTT-T was furnished in 78% yield by refluxing the CHO-terminated IDTT derivative **1** with thiobarbituric acid derivative **2** in the presence of pyridine in $CHCl_3$ (Scheme 1). The detailed synthesis protocol of IDTT-T acceptor is included in the Supporting Information, and the ^1H NMR and ^{13}C NMR spectra of **IDTT-T** are shown in Figures S1 and S2, respectively.

To understand how the end group and backbone structure affects the orbital energy levels, cyclic voltammetry (CV) was carried out for ITIC and IDTT-T solutions in $CHCl_3$ using a

Scheme 1. (a) Structural Formulas of Low-Bandgap NFA ITIC and the New Medium-Bandgap NFA IDTT-T, (b) Molecular Structure of the Low-Bandgap Donor Polymer PTB7-th, and (c) Synthetic Scheme of IDTT-T

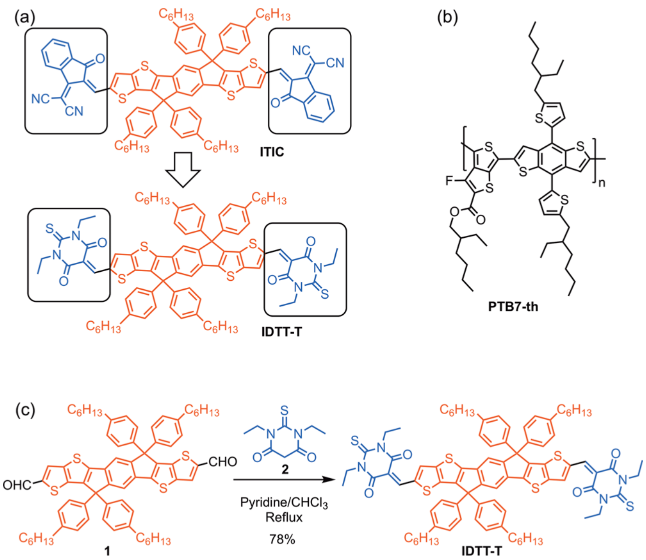

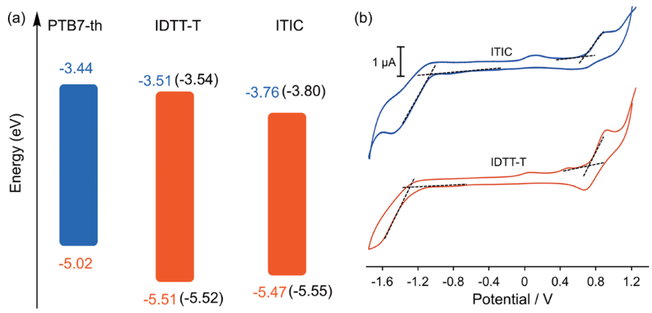

Figure 1. (a) Energy diagram of NFAs and their relative alignment to the energy levels of PTB7-th. The numbers in parentheses are from molecular modeling. (b) CVs of IDTT-T and ITIC (referenced to Fc/Fc+ redox couple. Scan rate: 100 mV/s).

three-electrode setup and ferrocene as the internal standard. The ionization potentials and electron affinities, which are also widely termed HOMO and LUMO energy levels, were estimated to be −5.47 and −3.76 eV for ITIC and −5.51 eV and −3.51 eV for IDTT-T, respectively, based on the corresponding onset potential of the first oxidative and reductive wave (Figures 1b and S3 and Table S1). While the variation of HOMO levels was negligible between the two NFAs, the 0.25 eV higher LUMO energy level of IDTT-T compared to ITIC reflected the significantly weaker electron-withdrawing ability of TBA end group than the cyano indone group and is consistent with the modeling results. When combined with the PTB7-th polymer donor,[55] the ΔE_{DA} shows a significant increase from 1.26 eV for the low-bandgap ITIC acceptor to 1.51 eV for the medium-gap IDTT-T, which alludes to a higher V_{OC} in OPV devices.

The end group modulation on energy levels correlates well with the absorption properties. As shown in Figure 2a, the absorption edge of IDTT-T shows a significant blue shift of 86 nm compared to that of ITIC, in accordance with an optical bandgap increase from 1.71 eV for ITIC to 2.00 eV for IDTT-T. The absorption spectrum of ITIC has a large overlap with

DOI: 10.1021/acsenergylett.8b00366
ACS Energy Lett. XXXX, XXX, XXX−XXX

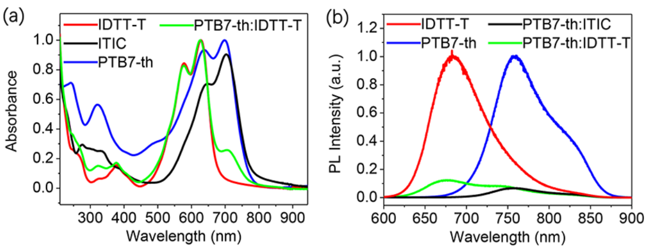

Figure 2. Absorption and photoluminescence spectra of PTB7-th and NFA films: (a) absorption spectra of pristine PTB7-th, ITIC, IDTT-T, and PTB7-th:IDTT-T blend film with a composition ratio of 1:2; (b) photoluminescence spectra of pristine PTB7-th, IDTT-T, PTB7-th:ITIC, and PTB7-th:IDTT-T blend films with a composition ratio of 1:2.

that of the donor PTB7-th, leading to incomplete spectral coverage below 635 nm. In contrast, the IDTT-T absorption shows great complementarity to that of PTB7-th and better coverage between 450 and 650 nm, which is advantageous for photocurrent generation. As illustrated in Figure S4, IDTT-T also has a higher extinction coefficient than PTB7-th. It is noteworthy that the LUMO energy level of the TBA-terminated IDTT-T is among the highest for large bandgap NFA featuring similar A−D−A or A−π−D−π−A structures.[5,47,56−58]

Steady-state photoluminescence (PL) spectra of both pristine and PTB7-th:NFA blend films were obtained to examine the PL quenching efficiency, which is related to the exciton dissociation and photoinduced charge-transfer properties of the donor−acceptor pairs. The pristine PTB7-th film exhibited a PL peak at ∼758 nm (Figure 2b). When blended with IDTT-T in a donor:acceptor ratio of 1:2, the photoluminescence was quenched by ∼94%. Comparable PL quenching efficiency was observed for the ITIC:PTB7-th blend, indicating similar exciton dissociation in PTB7-th:NFAs.[59] In other words, despite the reduction of the LUMO offset between the donor and acceptor, lifting LUMO energy levels of non-fullerene acceptors to increase ΔE_{DA} has a negligible impact on the charge-transfer efficiency and photocurrent generation. The PTB7-th:IDTT-T film displays an additional PL peak at ∼675 nm, which should be ascribed to the residual emission of IDTT-T (Figure 2b).

Photovoltaic devices based on the inverted structure (ITO/ZnO/PTB7-th:NFA (1:2)/MoO_3/Ag) were fabricated to verify the variation of V_{OC} for different NFAs. As shown in Figure 3a, the prototype PTB7-th:ITIC device displayed a V_{OC} of 0.828 V, a J_{SC} of 14.4 mA/cm^2, a fill factor (FF) of 67%, and a PCE of 8.0%, which are comparable to those of conventional PTB7-th:fullerene-based OPVs.[60] For the IDTT-T based devices, the

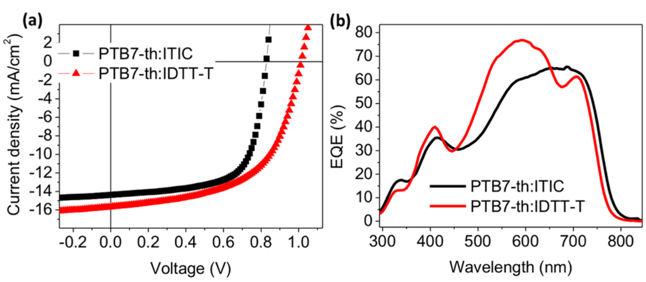

Figure 3. Photovoltaic performance for two different NFAs (PTB7-th:ITIC and PTB7-th:IDTT-T) based devices: (a) *J*−*V* curves under illumination of 100 mW/cm^2, AM 1.5G; (b) EQE curves.

V_{OC} was increased to 1.015 V, together with a FF of 57% and a significantly enhanced J_{SC} of 15.7 mA/cm^2, leading to a high PCE of 9.0%. Table 1 displays average device parameters for

Table 1. Average Device Parameters for Two Different NFAs (PTB7-th:ITIC and PTB7-th:IDTT-T) Based Devices

D:A	V_{OC} (V)	J_{SC} (mA/cm^2)	FF (%)	PCE (%)	R_{se}[a] (Ω)	R_{sh}[b] (Ω)
PTB7-th:ITIC	0.825	14.4	66	7.8	2.3	15.6
PTB7-th:IDTT-T	1.01	15.7	57	9.1	4.9	12.5

[a]Series resistance. [b]Shunt resistance.

two different NFAs (PTB7-th:ITIC and PTB7-th:IDTT-T) based devices and shows that the average PCE was around 7.8% and 9.1%, respectively. The devices based on PTB7-th:IDTT-T films exhibited a larger series resistance, which was consistent with the lower FF. The larger series resistance is attributable to a rougher surface [shown later by atomic force microscopy (AFM) characterization] or the presence of more voids for more shorting channels (current-leaking), which is further indicated by the smaller shunt resistance. Further optimization of the film morphology should reduce series resistance and increase shunt resistance for higher FF and better device performance. The high V_{OC} corresponds to a very low energy loss, E_{loss}, of 0.57 eV, which was calculated using the equation $E_{loss} = E_g - eV_{OC}$,[61,62] where E_g is the optical bandgap of PTB7-th, the active material with the smallest bandgap. Figure 3b displays external quantum efficiency (EQE) spectra that were acquired from different NFA-based devices. The variation of the calculated J_{SC} by the integration of the EQE spectra with solar spectrum AM 1.5G (100 mW/cm^2) is consistent with the variation of the measured J_{SC}. The shift of cutoff edge of EQE curves (Figure 3b) agrees well with the blue shift of the absorption edge of NFA materials (Figure 2a). Significant enhancement between ∼450 and 650 nm for the PTB7-th:IDTT-T device should be attributed to the characteristic absorption feature from the medium-bandgap IDTT-T, serving as a complementary absorber to that of the low-bandgap PTB7-th polymer donor.

Motivated by the superior photovoltaic performance of IDTT-T over ITIC when paired with PTB7-th, further optimization of the PTB7-th:IDTT-T device performance was carried out under various conditions. It was found that thermal annealing treatment of the active layer films resulted in negligible improvement in device performance (Figure S5); therefore, no thermal treatment was exerted in further optimization. A thickness-dependent study of photovoltaic performance in both standard structure (ITO/PEDOT:PSS/PTB7-th:IDTT-T/Ca/Al) and inverted structure (ITO/ZnO/PTB7-th:IDTT-T/MoO_3/Ag) devices (Figure 4a,b) indicated that the inverted devices exhibited photovoltaic performance superior to that of the conventional counterparts, consistent with previous reports.[63,64] For the 57 nm thick PTB7-th:IDTT-T device, the inverted device showed a PCE of 9.1%, whereas the conventional counterpart exhibited only 6.1%. Additionally, the V_{OC} of 1.01 V in the inverted device was higher than the V_{OC} of 0.888 V in the conventional counterpart. However, the thicker active layer (e.g., 78 and 110 nm) led to decrease in photovoltaic performance in both conventional and inverted devices. With the optimal thickness of 57 nm, we subsequently carried out the study of photovoltaic performance as a function

DOI: 10.1021/acsenergylett.8b00366
ACS Energy Lett. XXXX, XXX, XXX−XXX

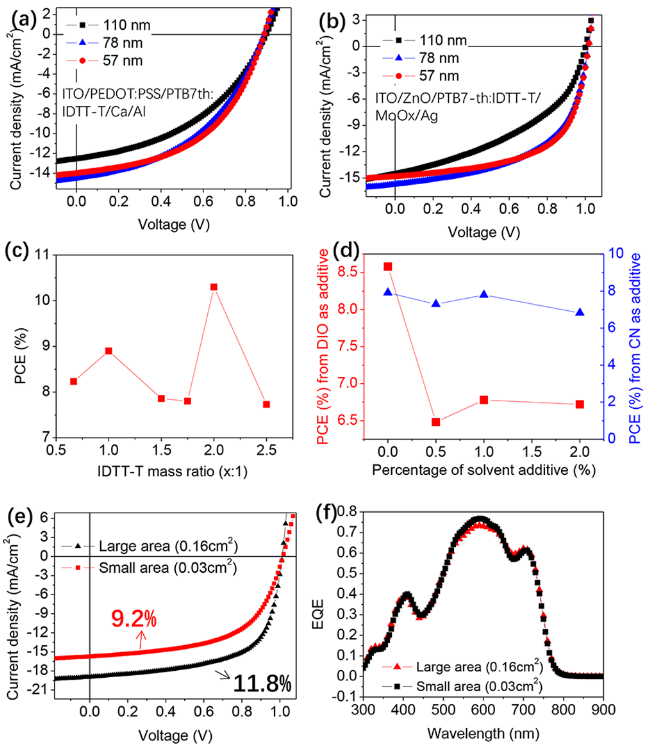

Figure 4. Optimization of photovoltaic performances: *J*−*V* curves acquired from devices based on the PTB7-th:IDTT-T active layer in (a) conventional structure (ITO/PEDOT:PSS/PTB7-th:IDTT-T/Ca/Al) and (b) inverted structure (ITO/ZnO/PTB7-th:IDTT-T/MoOx/Ag) device; variation in PCE as a function of (c) composition ratio between IDTT-T and PTB7-th; and (d) percentage of solvent additives [blue triangles, chloronaphthalene (CN); red squares, 1,8-diiodooctane (DIO)]; (e) *J*−*V* curves of the highest-performance cells with different device areas under illumination of 100 mW/cm^2; (f) corresponding EQE curves for devices in panel e.

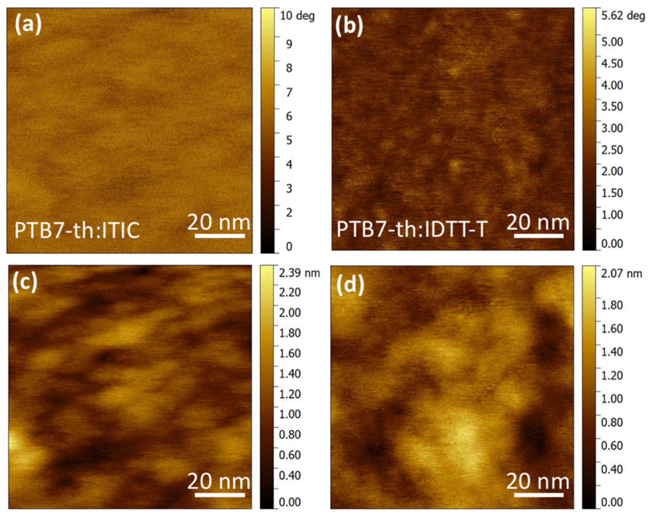

Figure 5. Atomic force microscopic (AFM) phase (a and b) and amplitude (c and d) images of PTB7-th:ITIC (a and c) and PTB7-th:IDTT-T (b and d) blend films with a composition ratio of 1:2.

of IDTT-T:PTB7-th composition ratio in the active layer. It was found that the devices with a donor:acceptor ratio of 1:2 showed the highest PCE of 10.3% (Figure 4c). The solvent additives, such as chloronaphthalene (CN) and 1,8-diiodooctane (DIO), played a negative effect to give decreased PCE (Figure 4d), which is different from previously reported results.[14,65−67] Considering the above optimal fabrication conditions, we fabricated both large-area (0.16 cm^2) and small-area (0.03 cm^2) devices, which yielded the highest PCEs of 9.2% and 11.8% with V_{OCs} of 1.01 V, respectively (Figure 4e). A histogram of the device efficiencies is plotted in Figure S6. The variation in J_{SC} values for different device areas is consistent with the variation in the calculated J_{SC} based on the EQE curves (Figure 4f). The high V_{OC} of over 1 V in our devices is among the highest for high-efficiency (over 10%) NFA OPVs.[68,69]

The AFM phase and amplitude images were obtained to examine nanoscale phase morphology in the blend films of PTB7-th:ITIC (Figure 5a,c) and PTB7-th:IDTT-T (Figure 5b,d). The amplitude images show similar surface roughness of 0.230 and 0.300 nm for PTB7-th:ITIC (Figure 5c) and PTB7-th:IDTT-T (Figure 5d), respectively. The phase contrast between PTB7-th and ITIC domains is invisible for the PTB7-th:ITIC blend film (Figure 5a), most likely because of the similar elastic properties of PTB7-th and ITIC materials, leading to the similar phase angle change with respect to the AFM cantilever.[11] For the PTB7-th:IDTT-T (Figure 5b) film, the obviously improved phase contrast of the donor and acceptor domains indicates the enhanced phase separation that is beneficial for improved exciton dissociation and photo-induced charge transfer.

Grazing incident wide-angle X-ray scattering (GIWAXS) studies were conducted to further reveal the molecular packing behavior in the thin films of individual components and the blends. The ITIC (Figure 6a) and IDTT-T (Figure 6b) films displayed varying degrees of crystallinity in the horizontal (100) plane, with the former showing a more discernible (010) out-of-plane diffraction peak that suggests "face-on" oriented crystallites. The GIWAXS pattern of PTB7-th (Figure 6c) signified that the PTB7-th polymers form crystallites with a preferred face-on orientation. In the two blended polymer:NFA films (Figure 6d,e), the preferential "face-on" orientations of the PTB7-th polymer donor was maintained, meanwhile both the in-plane peaks and the out-of-plane peaks of the NFAs disappeared, as can be seen from the vertical and horizontal linecuts (Figure 6g,h). The decreased crystallinity was in accordance with good blending between the polymer and the NFA small molecules, a prerequisite for the formation of favorable phase separation at the nanoscale for efficient charge separation.[70] The very similar patterns for the ITIC and IDTT-T blend films also suggested that the end groups in NFAs have little impact on molecular orientation and packing behavior, thus implying that the thin film morphology does not account for the simultaneous enhancement of both V_{OC} and J_{SC}. In addition, thermal annealing of the PTB7-th:IDTT-T film induced no notable changes of the GIWAXS pattern (Figure 6f), which suggests that the nanoscale morphology was thermally stable under such conditions. This thermal behavior agrees well with the observation of very similar device performances before and after thermal treatment, which also indicates good device stability.

In order to understand how the end groups in NFAs impact charge transport properties, the space charge limited current (SCLC) method was applied to estimate electron and hole mobilities in the PTB7-th:ITIC and PTB7-th:IDTT-T blend films. The *J*−*V* curves (measured in the dark) of both electron-only and hole-only devices are shown in Figure S7. By fitting

DOI: 10.1021/acsenergylett.8b00366
ACS Energy Lett. XXXX, XXX, XXX−XXX

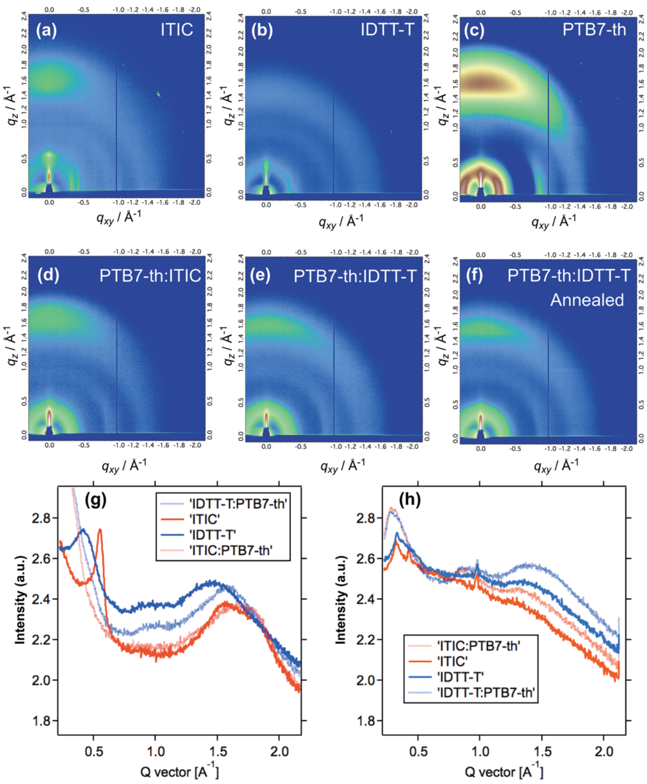

Figure 6. 2D GIWAXS patterns of pristine films (a) ITIC, (b) IDTT-T, and (c) PTB7-th and blend films (d) PTB7-th:ITIC, (e) PTB7-th:IDTT-T, and (f) PTB7-th:IDTT-T (thermally annealed at 100 °C for 10 min). (g) Vertical and (h) horizontal linecuts of the pure NFA films and their blends with PTB7-th.

the $J-V$ curves with the SCLC model,[71,72] we found that the electron and hole mobilities of the PTB7-th:ITIC blend film were 2.43×10^{-4} and 2.07×10^{-2} cm^2/(V s) (Table 2), respectively. When using end-group-modified IDTT-T to replace ITIC in the blend films, the electron and hole mobilities of the blend film were determined to be 3.98×10^{-3} and 5.19×10^{-3} cm^2/(V s), respectively, showing not only an increased electron mobility but also clearly more balanced electron and hole transport than those of the PTB7-th:ITIC blend film. Balanced carrier transport is important for reducing bimolecular recombination and also improves charge collection at the respective electrodes. As a result, J_{SC} was considerably improved in the corresponding devices (Figure 3a).

Table 2. Electron and Hole Mobilities in PTB7-th:ITIC and PTB7-th:IDTT-T Blend Films Estimated by the Space Charge Limited Current (SCLC) Method

material	μ_e (cm^2/(V s))	μ_h (cm^2/(V s))
PTB7-th:ITIC	2.43×10^{-4}	2.07×10^{-2}
PTB7-th:IDTT-T	3.98×10^{-3}	5.19×10^{-3}

We present a high-performance medium-bandgap nonfullerene acceptor that features an optical bandgap of 2.0 eV and a high LUMO energy level. The combined use of a weakly electron-withdrawing TBA end group and the IDTT core in an A−D−A geometry gives rise to IDTT-T with a significantly raised LUMO energy level compared to ITIC, together with absorption in the bluer region of the visible spectrum that matches well with that of the low-bandgap PTB7-th donor. Because of the high LUMO level and the complementary absorption properties, the OPV devices using PTB7-th:IDTT-T as the active layer showcase a high V_{OC} over 1 V, together with a high J_{sc}, low energy loss, and a highest PCE reaching 11.8% in lab-scale devices. This performance compares favorably to the performance of other wider gap NFAs reported to-date (Table S2).[15−18] While the current OPV devices with leading efficiencies are still based on low-bandgap NFAs,[36,43] which feature high photocurrent generation but often at the expense of V_{OC}, this work demonstrated that simultaneous increase of V_{OC} and photocurrent generation in bulk heterojunction OPVs can be realized by the use of judiciously designed wide bandgap NFAs and donor materials with proper spectrum overlap. The discovery of potent wide bandgap NFAs thus not only broadens the scope of the OPV material design landscape but also opens the door to high-efficiency OPV devices in new applications, such as multicomponent solar cells.

EXPERIMENTAL SECTION

Synthesis of ZnO. The ZnO nanoparticles were synthesized by a sol−gel method, modified from the procedure reported in the literature.[73] In a 20 mL vial, potassium hydroxide (94.4 mg, 1.7 mmol) was first dissolved in ethanol (10 mL); the solution was then sonicated and cooled to 0 °C using an ice bath. In a second 20 mL vial, zinc acetate dihydrate (220 mg, 1 mmol) was dissolved in ethanol (10 mL); the solution was then heated to 70 °C for up to 30 min or until all the zinc acetate dihydrate dissolved. Heating beyond the recommended time leads to precipitation of insoluble zinc acetate and should be avoided. Upon dissolution, the ZnAc solution was taken off the heat and then cooled at 0 °C for about a minute. The KOH solution was subsequently added into the ZnAc solution dropwise with stirring. The resulting clear solution was stored in a refrigerator overnight. The clear zinc oxide solution was transferred into two large falcon tubes. Zinc oxide nanoparticles were precipitated by adding hexanes (40 mL) in each tube followed by centrifuging for 15 min at 4000 rpm. The solution was decanted off, and the remaining ZnO pellet was redissolved in ethanol (10 mL) for further use.

Thin Film and Device Characterization. The $J-V$ curves were acquired in the dark and under illumination of one sun (AM 1.5G) with light intensity of 100 mW/cm^2. A standard Newport silicon diode was applied to calibrate the light intensity. EQE was measured by a home-built IPCE system. The absorption spectrum and photoluminscence spectrum were obtained by a Cary 5000 UV-vis-NIR spectrometer and a Horiba NanoLog spectrofluorometer, respectively. The excitation wavelength for PL measurement was 500 nm. An Asylum MFP-3D stand-alone AFM instrument from Oxford Instruments was used to take AFM images under tapping mode. GIWAXS patterns were acquired under X-ray incident angle of 0.14° and X-ray energy of 10 keV at Beamline 7.3.3 of the Advanced Light Source, Lawrence Berkeley National Laboratory.

Device Fabrication and Characterization. For the inverted device fabrication, the ZnO nanoparticle solution, filtered by a 0.25 μm filter, was spun-cast at 4000 rpm for 60 s on a clean ITO glass substrate and thermally annealed at 120 °C for 10 min in air. The concentration of the PTB7-th:NFA (composition ratio = 1:2) solution was 25 mg/mL, dissolved in chlorobenzene. The solution was spun-coated on the ZnO layer at 3000 rpm for 40 s in a N_2-filled glovebox. The 8 nm thick MoO_3 and 100 nm thick Ag layers were subsequently prepared by thermal evaporation. For the standard device

DOI: 10.1021/acsenergylett.8b00366
ACS Energy Lett. XXXX, XXX, XXX−XXX

fabrication, the active layer fabrication was the same as that for the inverted device, and the only differences were (1) the hole transport layer PEDOT:PSS (P4083), which was spun-coated on ITO glass at 4000 rpm followed by a thermal annealing treatment of 135 °C for 20 min, and (2) the cathode calcium (20 nm) and aluminum (100 nm) prepared by thermal evaporation under vacuum condition (2×10^{-6} mbar). Both large-area (0.16 cm^2) and small-area (0.03 cm^2) devices were fabricated.

■ ASSOCIATED CONTENT

Supporting Information

The Supporting Information is available free of charge on the ACS Publications website at DOI: 10.1021/acsenergylett.8b00366.

Synthesis details and additional optical, electrochemical, and device characterization data (PDF)

■ AUTHOR INFORMATION

Corresponding Authors

*E-mail: yliu@lbl.gov.
*E-mail: yangb1@hnu.edu.cn.

ORCID

Bo He: 0000-0003-1444-4625
Yi Liu: 0000-0002-3954-6102

Author Contributions

‡B.H. and B.Y. contributed equally.

Notes

The authors declare no competing financial interest.

■ ACKNOWLEDGMENTS

This work was performed at the Molecular Foundry, and the X-ray experiments were conducted at the Advanced Light Source (ALS), Lawrence Berkeley National Laboratory, all of which are supported by the Office of Science, Office of Basic Energy Sciences, of the U.S. Department of Energy under Contract No. DE-AC02-05CH11231.

■ REFERENCES

(1) Li, G.; Shrotriya, V.; Huang, J.; Yao, Y.; Moriarty, T.; Emery, K.; Yang, Y. High-Efficiency Solution Processable Polymer Photovoltaic Cells by Self-Organization of Polymer Blends. *Nat. Mater.* **2005**, *4*, 864−868.

(2) Shaheen, S. E.; Brabec, C. J.; Sariciftci, N. S.; Padinger, F.; Fromherz, T.; Hummelen, J. C. 2.5% Efficient Organic Plastic Solar Cells. *Appl. Phys. Lett.* **2001**, *78*, 841−843.

(3) Heeger, A. J. 25th Anniversary Article: Bulk Heterojunction Solar Cells: Understanding the Mechanism of Operation. *Adv. Mater.* **2014**, *26*, 10−28.

(4) Cheng, Y. J.; Yang, S. H.; Hsu, C. S. Synthesis of Conjugated Polymers for Organic Solar Cell Applications. *Chem. Rev.* **2009**, *109*, 5868−5923.

(5) Chen, W.; Zhang, Q. Recent Progress in Non-Fullerene Small Molecule Acceptors in Organic Solar Cells (OSCs). *J. Mater. Chem. C* **2017**, *5*, 1275−1302.

(6) He, Z.; Zhong, C.; Huang, X.; Wong, W. Y.; Wu, H.; Chen, L.; Su, S.; Cao, Y. Simultaneous Enhancement of Open−Circuit Voltage, Short−Circuit Current Density, and Fill Factor in Polymer Solar Cells. *Adv. Mater.* **2011**, *23*, 4636−4643.

(7) Elumalai, N. K.; Uddin, A. Open Circuit Voltage of Organic Solar Cells: an In-Depth Review. *Energy Environ. Sci.* **2016**, *9*, 391−410.

(8) Eckstein, B. J.; Melkonyan, F. S.; Zhou, N.; Manley, E. F.; Smith, J.; Timalsina, A.; Chang, R. P. H.; Chen, L. X.; Facchetti, A.; Marks, T. J. Buta-1,3-diyne-Based π-Conjugated Polymers for Organic Transistors and Solar Cells. *Macromolecules* **2017**, *50*, 1430−1441.

(9) Liu, J.; Liu, F.; Ding, Z.; Wang, L. An Organoboron Compound with Wide Absorption Spectrum for Organic Solar Cell Application. *Chem. Commun.* **2017**, *53*, 12213−12216.

(10) Yang, B.; Yuan, Y.; Sharma, P.; Poddar, S.; Korlacki, R.; Ducharme, S.; Gruverman, A.; Saraf, R.; Huang, J. Tuning the Energy Level Offset between Donor and Acceptor with Ferroelectric Dipole Layers for Increased Efficiency in Bilayer Organic Photovoltaic Cells. *Adv. Mater.* **2012**, *24*, 1455−1460.

(11) Wang, G.; Eastham, N. D.; Aldrich, T. J.; Ma, B.; Manley, E. F.; Chen, Z.; Chen, L.; Olvera, M.; Chang, R.; Melkonyan, F.; et al. Photoactive Blend Morphology Engineering through Systematically Tuning Aggregation in All−Polymer Solar Cells. *Adv. Energy Mater.* **2018**, 1702173.

(12) Kwon, O. K.; Uddin, M. A.; Park, J. H.; Park, S. K.; Nguyen, T. L.; Woo, H. Y.; Park, S. Y. A High Efficiency Nonfullerene Organic Solar Cell with Optimized Crystalline Organizations. *Adv. Mater.* **2016**, *28*, 910−916.

(13) Blom, P. W. M.; Mihailetchi, V. D.; Koster, L. J. A.; Markov, D. E. Device Physics of Polymer:Fullerene Bulk Heterojunction Solar Cells. *Adv. Mater.* **2007**, *19*, 1551−1566.

(14) Perez, L. A.; Rogers, J. T.; Brady, M. A.; Sun, Y.; Welch, G. C.; Schmidt, K.; Toney, M. F.; Jinnai, H.; Heeger, A. J.; Chabinyc, M. L.; et al. The Role of Solvent Additive Processing in High Performance Small Molecule Solar Cells. *Chem. Mater.* **2014**, *26*, 6531−6541.

(15) Tang, A.; Xiao, B.; Wang, Y.; Gao, F.; Tajima, K.; Bin, H.; Zhang, Z.-G.; Li, Y.; Wei, Z.; Zhou, E. Simultaneously Achieved High Open-Circuit Voltage and Efficient Charge Generation by Fine-Tuning Charge-Transfer Driving Force in Nonfullerene Polymer Solar Cells. *Adv. Funct. Mater.* **2018**, *28*, 1704507.

(16) Liu, Y.; Zhang, Z.; Feng, S. Y.; Li, M.; Wu, L. L.; Hou, R.; Xu, X. J.; Chen, X. B.; Bo, Z. S. Exploiting Noncovalently Conformational Locking as a Design Strategy for High Performance Fused-Ring Electron Acceptor Used in Polymer Solar Cells. *J. Am. Chem. Soc.* **2017**, *139*, 3356−3359.

(17) Hendsbee, A.; Sun, J.; Law, W.; Yan, H.; Hill, I.; Spasyuk, D.; Welch, G. Synthesis, Self-Assembly, and Solar Cell Performance of *N*-Annulated Perylene Diimide Non-Fullerene Acceptors. *Chem. Mater.* **2016**, *28*, 7098−7109.

(18) Baran, D.; Ashraf, R. S.; Hanifi, D. A.; Abdelsamie, M.; Gasparini, N.; Röhr, J. A.; Holliday, S.; Wadsworth, A.; Lockett, S.; Neophytou, M.; et al. Reducing the Efficiency-Stability-Cost Gap of Organic Photovoltaics with Highly Efficient and Stable Small Molecule Acceptor Ternary Solar Cells. *Nat. Mater.* **2017**, *16*, 363−369.

(19) Aldrich, T. J.; Swick, S. M.; Melkonyan, F. S.; Marks, T. J. Enhancing Indacenodithiophene Acceptor Crystallinity via Substituent Manipulation Increases Organic Solar Cell Efficiency. *Chem. Mater.* **2017**, *29*, 10294−10298.

(20) Heumueller, T.; Mateker, W. R.; Distler, A.; Fritze, U. F.; Cheacharoen, R.; Nguyen, W. H.; Biele, M.; Salvador, M.; Delius, M. V.; Egelhaaf, H. J. Morphological and Electrical Control of Fullerene Dimerization Determines Organic Photovoltaic Stability. *Energy Environ. Sci.* **2016**, *9*, 247−256.

(21) Li, Y. Fullerene-Bisadduct Acceptors for Polymer Solar Cells. *Chem. - Asian J.* **2013**, *8*, 2316−2328.

(22) Zhao, W.; Qian, D.; Zhang, S.; Li, S.; Inganäs, O.; Gao, F.; Hou, J. Fullerene-Free Polymer Solar Cells with over 11% Efficiency and Excellent Thermal Stability. *Adv. Mater.* **2016**, *28*, 4734−4739.

(23) Zhang, X.; Lu, Z.; Ye, L.; Zhan, C.; Hou, J.; Zhang, S.; Jiang, B.; Zhao, Y.; Huang, J.; Zhang, S. A Potential Perylene Diimide Dimer−Based Acceptor Material for Highly Efficient Solution−Processed Non−Fullerene Organic Solar Cells with 4.03% Efficiency. *Adv. Mater.* **2013**, *25*, 5791−5797.

(24) Lin, Y.; Wang, J.; Zhang, Z. G.; Bai, H.; Li, Y.; Zhu, D.; Zhan, X. An Electron Acceptor Challenging Fullerenes for Efficient Polymer Solar Cells. *Adv. Mater.* **2015**, *27*, 1170−1174.

(25) Wu, Q.; Zhao, D.; Yang, J.; Sharapov, V.; Cai, Z.; Li, L.; Zhang, N.; Neshchadin, A.; Chen, W.; Yu, L. Propeller-Shaped Acceptors for

DOI: 10.1021/acsenergylett.8b00366
ACS Energy Lett. XXXX, XXX, XXX−XXX

High-Performance Non-Fullerene Solar Cells: Importance of Molecular Geometry Rigidity. *Chem. Mater.* **2017**, *29*, 1127−1133.

(26) Wang, Y.; Fan, Q.; Guo, X.; Li, W.; Guo, B.; Su, W.; Ou, X.; Zhang, M. High-Performance Nonfullerene Polymer Solar Cells Based on Fluorinated Wide Bandgap Copolymer with a High Open-Circuit Voltage of 1.04 V. *J. Mater. Chem. A* **2017**, *5*, 22180−22185.

(27) Hartnett, P. E.; Matte, H. S. S. R.; Eastham, N. D.; Jackson, N. E.; Wu, Y. L.; Chen, L. X.; Ratner, M. A.; Chang, R. P. H.; Hersam, M. C.; Wasielewski, M. R.; et al. Ring-Fusion as a Perylenediimide Dimer Design Concept for High-Performance Non-Fullerene Organic Photovoltaic Acceptors. *Chem. Sci.* **2016**, *7*, 3543−3555.

(28) McAfee, S. M.; Dayneko, S. V.; Josse, P.; Blanchard, P.; Cabanetos, C.; Welch, G. C. Simply Complex: The Efficient Synthesis of an Intricate Molecular Acceptor for High-Performance Air-Processed and Air-Tested Fullerene-Free Organic Solar Cells. *Chem. Mater.* **2017**, *29*, 1309−1314.

(29) Zhong, H.; Wu, C. H.; Li, C. Z.; Carpenter, J.; Chueh, C. C.; Chen, J. Y.; Ade, H.; Jen, A. K. Rigidifying Nonplanar Perylene Diimides by Ring Fusion Toward Geometry−Tunable Acceptors for High−Performance Fullerene−Free Solar Cells. *Adv. Mater.* **2016**, *28*, 951−958.

(30) Lin, Y. Z.; Wang, J. Y.; Dai, S. X.; Li, Y. F.; Zhu, D. B.; Zhan, X. W. A Twisted Dimeric Perylene Diimide Electron Acceptor for Efficient Organic Solar Cells. *Adv. Energy Mater.* **2014**, *4*, 1400420.

(31) Fei, Z.; Eisner, F. D.; Jiao, X.; Azzouzi, M.; Röhr, J. A.; Han, Y.; Shahid, M.; Chesman, A. R.; Easton, C. D.; McNeill, C. R.; et al. An Alkylated Indacenodithieno [3,2-b]Thiophene-Based Nonfullerene Acceptor with High Crystallinity Exhibiting Single Junction Solar Cell Efficiencies Greater than 13% with Low Voltage Losses. *Adv. Mater.* **2018**, *30*, 1705209.

(32) Lin, Y.; Wang, J.; Zhang, Z.-G.; Bai, H.; Li, Y.; Zhu, D.; Zhan, X. An Electron Acceptor Challenging Fullerenes for Efficient Polymer Solar Cells. *Adv. Mater.* **2015**, *27*, 1170−1174.

(33) Lin, Y.; He, Q.; Zhao, F.; Huo, L.; Mai, J.; Lu, X.; Su, C.-J.; Li, T.; Wang, J.; Zhu, J.; Sun, Y.; Wang, C.; Zhan, X. A Facile Planar Fused-Ring Electron Acceptor for as-Cast Polymer Solar Cells with 8.71% Efficiency. *J. Am. Chem. Soc.* **2016**, *138*, 2973−2976.

(34) Lin, Y.; Zhao, F.; He, Q.; Huo, L.; Wu, Y.; Parker, T. C.; Ma, W.; Sun, Y.; Wang, C.; Zhu, D.; Heeger, A. J.; Marder, S. R.; Zhan, X. High-Performance Electron Acceptor with Thienyl Side Chains for Organic Photovoltaics. *J. Am. Chem. Soc.* **2016**, *138*, 4955−4961.

(35) Li, Y.; Zhong, L.; Gautam, B.; Bin, H.-J.; Lin, J.-D.; Wu, F.-P.; Zhang, Z.; Jiang, Z.-Q.; Zhang, Z.-G.; Gundogdu, K.; Li, Y.; Liao, L.-S. A Near-Infrared Non-Fullerene Electron Acceptor for High Performance Polymer Solar Cells. *Energy Environ. Sci.* **2017**, *10*, 1610−1620.

(36) Zhao, W.; Li, S.; Yao, H.; Zhang, S.; Zhang, Y.; Yang, B.; Hou, J. Molecular Optimization Enables over 13% Efficiency in Organic Solar Cells. *J. Am. Chem. Soc.* **2017**, *139*, 7148−7151.

(37) Cui, Y.; Yao, H.; Gao, B.; Qin, Y.; Zhang, S.; Yang, B.; He, C.; Xu, B.; Hou, J. Fine-Tuned Photoactive and Interconnection Layers for Achieving over 13% Efficiency in a Fullerene-Free Tandem Organic Solar Cell. *J. Am. Chem. Soc.* **2017**, *139*, 7302−7309.

(38) Xue, L.; Yang, Y.; Xu, J.; Zhang, C.; Bin, H.; Zhang, Z.-G.; Qiu, B.; Li, X.; Sun, C.; Gao, L.; Yao, J.; Chen, X.; Yang, Y.; Xiao, M.; Li, Y. Side Chain Engineering on Medium Bandgap Copolymers to Suppress Triplet Formation for High-Efficiency Polymer Solar Cells. *Adv. Mater.* **2017**, *29*, 1703344.

(39) Liu, T.; Meng, D.; Cai, Y.; Sun, X.; Li, Y.; Huo, L.; Liu, F.; Wang, Z.; Russell, T. P.; Sun, Y. High-Performance Non-Fullerene Organic Solar Cells Based on a Selenium-Containing Polymer Donor and a Twisted Perylene Bisimide Acceptor. *Adv. Sci.* **2016**, *3*, 1600117.

(40) McAfee, S. M.; Payne, A.; Dayneko, S. V.; Kini, G. P.; Song, C. E.; Lee, J.; Welch, G. C. A Non-Fullerene Acceptor with a Diagnostic Morphological Handle for Streamlined Screening of Donor Materials in Organic Solar Cells. *J. Mater. Chem. A* **2017**, *5*, 16907−16913.

(41) Kim, T.; Kim, J. H.; Kang, T. E.; Lee, C.; Kang, H.; Shin, M.; Wang, C.; Ma, B.; Jeong, U.; Kim, T. S.; et al. Flexible, Highly Efficient All-Polymer Solar Cells. *Nat. Commun.* **2015**, *6*, 8547.

(42) Sun, D.; Meng, D.; Cai, Y.; Fan, B.; Li, Y.; Jiang, W.; Huo, L.; Sun, Y.; Wang, Z. Non-Fullerene-Acceptor-Based Bulk-Heterojunction Organic Solar Cells with Efficiency over 7. *J. Am. Chem. Soc.* **2015**, *137*, 11156−11162.

(43) Xiao, Z.; Jia, X.; Ding, L. Ternary Organic Solar Cells Offer 14% Power Conversion Efficiency. *Sci. Bull.* **2017**, *62*, 1562−1564.

(44) Wang, M.; Wang, H.; Yokoyama, T.; Liu, X.; Huang, Y.; Zhang, Y.; Nguyen, T.-Q.; Aramaki, S.; Bazan, G. C. High Open Circuit Voltage in Regioregular Narrow Band Gap Polymer Solar Cells. *J. Am. Chem. Soc.* **2014**, *136*, 12576−12579.

(45) Yang, B.; Guo, F.; Yuan, Y.; Xiao, Z.; Lu, Y.; Dong, Q.; Huang, J. Solution-Processed Fullerene-Based Organic Schottky Junction Devices for Large-Open-Circuit-Voltage Organic Solar Cells. *Adv. Mater.* **2013**, *25*, 572−577.

(46) Sullivan, P.; Schumann, S.; Da Campo, R.; Howells, T.; Duraud, A.; Shipman, M.; Hatton, R. A.; Jones, T. S. Ultra-High Voltage Multijunction Organic Solar Cells for Low-Power Electronic Applications. *Adv. Energy Mater.* **2013**, *3*, 239−244.

(47) Beaumont, N.; Cho, S. W.; Sullivan, P.; Newby, D.; Smith, K. E.; Jones, T. S. Boron Subphthalocyanine Chloride as an Electron Acceptor for High-Voltage Fullerene-Free Organic Photovoltaics. *Adv. Funct. Mater.* **2012**, *22*, 561−566.

(48) Ma, D.; Feng, S.; Zhang, J.; Kou, C.; Gong, X.; Li, Q.; Xu, X.; Yan, S.; Bo, Z. Non-Fullerene Small Molecular Acceptors with a Carbazole Core for Organic Solar Cells with High Open-Circuit Voltage. *Dyes Pigm.* **2017**, *146*, 293−299.

(49) Zhang, Y.; Guo, X.; Guo, B.; Su, W.; Zhang, M.; Li, Y. Nonfullerene Polymer Solar Cells Based on a Perylene Monoimide Acceptor with a High Open−Circuit Voltage of 1.3 V. *Adv. Funct. Mater.* **2017**, *27*, 1603892.

(50) Cheng, P.; Zhang, M.; Lau, T. K.; Wu, Y.; Jia, B.; Wang, J.; Yan, C.; Qin, M.; Lu, X.; Zhan, X. Realizing Small Energy Loss of 0.55 eV, High Open−Circuit Voltage > 1 V and High Efficiency > 10% in Fullerene−Free Polymer Solar Cells via Energy Driver. *Adv. Mater.* **2017**, *29*, 1605216.

(51) Li, S.; Liu, W.; Li, C. Z.; Lau, T. K.; Lu, X.; Shi, M.; Chen, H. A Non-Fullerene Acceptor with a Fully Fused Backbone For Efficient Polymer Solar Cells with a High Open-Circuit Voltage. *J. Mater. Chem. A* **2016**, *4*, 14983−14987.

(52) Sun, J.; Zhang, Z.; Yin, X.; Zhou, J.; Yang, L.; Geng, R.; Zhang, F.; Zhu, R.; Yu, J.; Tang, W. High Performance Non-Fullerene Polymer Solar Cells Based on PTB7-Th as the Electron Donor with 10.42% Efficiency. *J. Mater. Chem. A* **2018**, *6*, 2549−2554.

(53) Liu, J.; Chen, S.; Qian, D.; Gautam, B.; Yang, G.; Zhao, J.; Bergqvist, J.; Zhang, F.; Ma, W.; Ade, H.; Inganäs, O.; Gundogdu, K.; Gao, F.; Yan, H. Fast Charge Separation in a Non-Fullerene Organic Solar Cell with a Small Driving Force. *Nat. Energy* **2016**, *1*, 16089.

(54) Ye, L.; Sun, K.; Jiang, W.; Zhang, S.; Zhao, W.; Yao, H.; Wang, Z.; Hou, J. Enhanced Efficiency in Fullerene-Free Polymer Solar Cell by Incorporating Fine-designed Donor and Acceptor Materials. *ACS Appl. Mater. Interfaces* **2015**, *7*, 9274−9280.

(55) Ding, Z.; Long, X.; Dou, C.; Liu, J.; Wang, L. A Polymer Acceptor with an Optimal LUMO Energy Level for All-Polymer Solar Cells. *Chem. Sci.* **2016**, *7*, 6197−6202.

(56) Li, Z.; Jiang, K.; Yang, G.; Lai, J. Y. L.; Ma, T.; Zhao, J.; Ma, W.; Yan, H. Donor Polymer Design Enables Efficient Non-Fullerene Organic Solar Cells. *Nat. Commun.* **2016**, *7*, 13094.

(57) Wen, S.; Wu, Y.; Wang, Y.; Li, Y.; Liu, L.; Jiang, H.; Liu, Z.; Yang, R. Pyran-Bridged Indacenodithiophene: A Novel Building Block for Constructing Efficient A-D-A Type Nonfullerene Acceptor for Polymer Solar Cells. *ChemSusChem* **2018**, *11*, 360−366.

(58) Lim, E. Two A−D−A−Type Non−Fullerene Small Molecule Acceptors Based on 1,3−Dimethylbarbituric Acid for OPVs. *B. Kor. Chem. Soc.* **2017**, *38*, 285−288.

(59) Clarke, T. M.; Ballantyne, A.; Shoaee, S.; Ying, W. S.; Duffy, W.; Heeney, M.; Mcculloch, I.; Nelson, J.; Durrant, J. R. Analysis of Charge Photogeneration as a Key Determinant of Photocurrent Density in Polymer: Fullerene Solar Cells. *Adv. Mater.* **2010**, *22*, 5287−5291.

DOI: 10.1021/acsenergylett.8b00366
ACS Energy Lett. XXXX, XXX, XXX−XXX

(60) Liao, S.-H.; Jhuo, H.-J.; Cheng, Y.-S.; Chen, S.-A. Fullerene Derivative-Doped Zinc Oxide Nanofilm as the Cathode of Inverted Polymer Solar Cells with Low-Bandgap Polymer (PTB7-Th) for High Performance. *Adv. Mater.* **2013**, *25*, 4766−4771.

(61) Ran, N. A.; Love, J. A.; Takacs, C. J.; Sadhanala, A.; Beavers, J. K.; Collins, S. D.; Huang, Y.; Wang, M.; Friend, R. H.; Bazan, G. C.; et al. Harvesting the Full Potential of Photons with Organic Solar Cells. *Adv. Mater.* **2016**, *28*, 1482−1488.

(62) Veldman, D.; Meskers, S. C. J.; Janssen, R. A. J. The Energy of Charge−Transfer States in Electron Donor-Acceptor Blends: Insight into the Energy Losses in Organic Solar Cells. *Adv. Funct. Mater.* **2009**, *19*, 1939−1948.

(63) Hu, X.; Yi, C.; Wang, M.; Hsu, C.-H.; Liu, S.; Zhang, K.; Zhong, C.; Huang, F.; Gong, X.; Cao, Y. High-Performance Inverted Organic Photovoltaics with over 1-μm Thick Active Layers. *Adv. Energy Mater.* **2014**, *4*, 1400378.

(64) Sun, Y.; Seo, J. H.; Takacs, C. J.; Seifter, J.; Heeger, A. J. Inverted Polymer Solar Cells Integrated with a Low-Temperature-Annealed Sol-Gel-Derived ZnO Film as an Electron Transport Layer. *Adv. Mater.* **2011**, *23*, 1679−1683.

(65) Lou, S. J.; Szarko, J. M.; Xu, T.; Yu, L.; Marks, T. J.; Chen, L. X. Effects of Additives on the Morphology of Solution Phase Aggregates Formed by Active Layer Components of High-Efficiency Organic Solar Cells. *J. Am. Chem. Soc.* **2011**, *133*, 20661−20663.

(66) Sharenko, A.; Gehrig, D.; Laquai, F.; Nguyen, T.-Q. The Effect of Solvent Additive on the Charge Generation and Photovoltaic Performance of a Solution-Processed Small Molecule:Perylene Diimide Bulk Heterojunction Solar Cell. *Chem. Mater.* **2014**, *26*, 4109−4118.

(67) Eastham, N. D.; Logsdon, J. L.; Manley, E. F.; Aldrich, T. J.; Leonardi, M. J.; Wang, G.; Powers-Riggs, N. E.; Young, R. M.; Chen, L. X.; Wasielewski, M. R.; et al. Hole-Transfer Dependence on Blend Morphology and Energy Level Alignment in Polymer: ITIC Photovoltaic Materials. *Adv. Mater.* **2018**, *29*, 1704263.

(68) Chen, S.; Liu, Y.; Lin, Z.; Chow, P. C. Y.; Zheng, W.; Zhang, G.; Wei, M.; He, Y. A Wide-Bandgap Donor Polymer for Highly Efficient Non-Fullerene Organic Solar Cells with a Small Voltage Loss. *J. Am. Chem. Soc.* **2017**, *139*, 6298−6301.

(69) Baran, D.; Kirchartz, T.; Wheeler, S.; Dimitrov, S.; Abdelsamie, M.; Gorman, J.; Ashraf, R.; Holliday, S.; Wadsworth, A.; Gasparini, N.; et al. Reduced Voltage Losses Yield 10% and > 1V Fullerene Free Organic Solar Cells. *Energy Environ. Sci.* **2016**, *9*, 3783−3793.

(70) Wei, Z.; Xi, H.; Dong, H.; Wang, L.; Xu, W.; Hu, W.; Zhu, D. Blending Induced Stack-Ordering and Performance Improvement in a Solution-Processed *n*-Type Organic Field-Effect Transistor. *J. Mater. Chem.* **2010**, *20*, 1203−1207.

(71) Faist, M. A.; Shoaee, S.; Tuladhar, S.; Dibb, G. F. A.; Foster, S.; Gong, W.; Kirchartz, T.; Bradley, D. D. C.; Durrant, J. R.; Nelson, J. Understanding the Reduced Efficiencies of Organic Solar Cells Employing Fullerene Multiadducts as Acceptors. *Adv. Energy Mater.* **2013**, *3*, 744−752.

(72) Yang, B.; Cox, J.; Yuan, Y.; Guo, F. Increased Efficiency of Low Band Gap Polymer Solar Cells at Elevated Temperature and Its Origins. *Appl. Phys. Lett.* **2011**, *99*, 133302.

(73) Tan, M. J.; Zhong, S.; Li, J.; Chen, Z.; Chen, W. Air-Stable Efficient Inverted Polymer Solar Cells Using Solution-Processed Nanocrystalline ZnO Interfacial Layer. *ACS Appl. Mater. Interfaces* **2013**, *5*, 4696−4701.

DOI: 10.1021/acsenergylett.8b00366
ACS Energy Lett. XXXX, XXX, XXX−XXX